A WORKSHOP ON

MICROSTRUCTURE SENSORS IN THE OCEAN

PROCEEDINGS
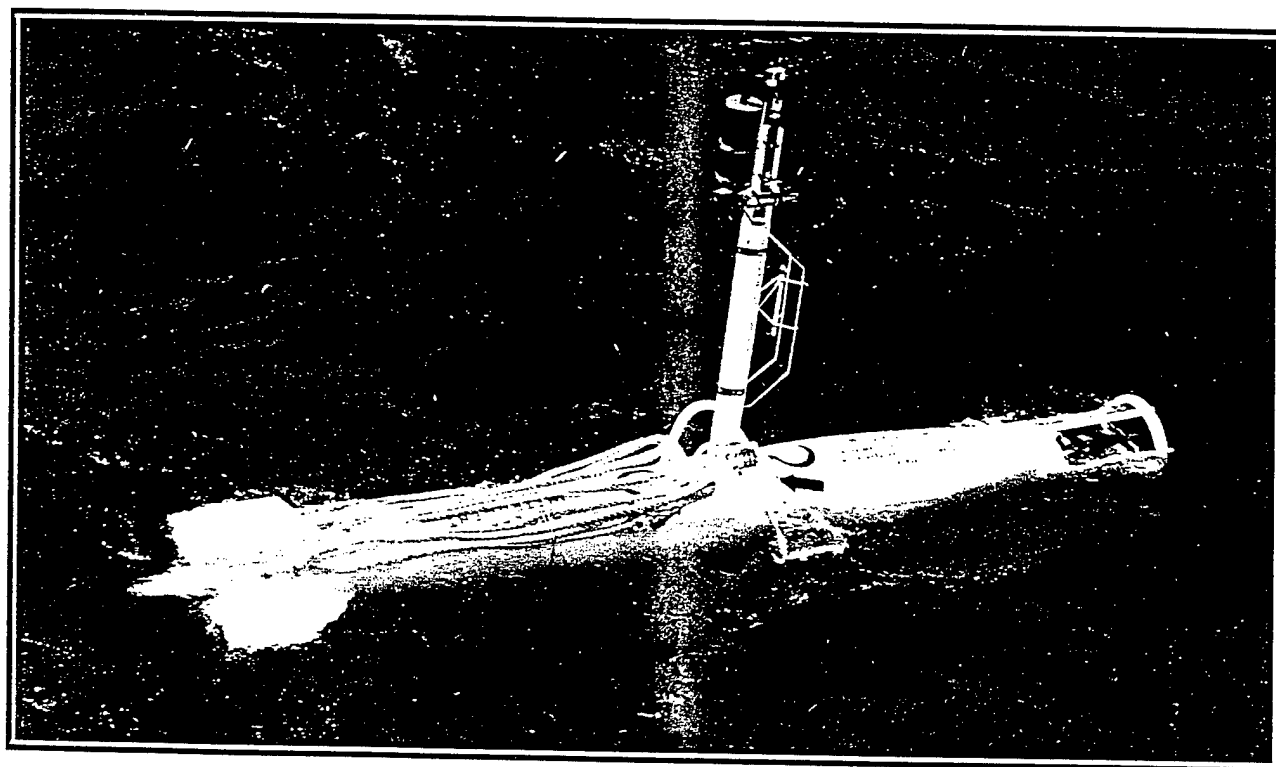
Sponsored by

Office of Naval Research
Arlington, VA

19970303 135

PROCEEDINGS

MICROSTRUCTURE SENSORS WORKSHOP

23-25 October 1996

Timberline Lodge, Mt. Hood
Oregon, U.S.A.

Measurement of the Microstructure of Ocean Surface Roughness

Paul. A. Hwang

Code 7332, Naval Research Laboratory

Stennis Space Center, MS 39529 USA

Abstract - This paper describes a technique to measure the spatial structure of short capillary-gravity waves in the ocean. The method is based on optical refraction of a single laser beam crossing the air-water interface to derived the surface slope information. By quickly scanning the laser beam, the spatial and temporal evolution of the surface undulation can be studied in great detail. The spatial measurement of the surface fluctuation also allows direct computation of the wavenumber spectrum in the capillary-gravity wave regime to avoid the difficulty of resolving the Doppler frequency shift as encountered in the processing of high frequency spectra derived from a single-point sensor.

1. INTRODUCTION

For ocean remote sensing, short capillary-gravity (CG) waves on the water surface serve as the roughness elements to scatter back the radar waves. Unlike solid scatterers, CG waves constantly undergo dynamic changes, subject to external wind forcing, breaking and viscous dissipation, and turbulence interaction. These waves/scatterers are convected and refracted by surface currents, at the same time advecting with their own group velocities that are wavelength-dependent. In addition to these kinematic changes, the spatial and temporal distribution of CG waves are modified dynamically by the surface currents through modulation process. Because the mechanisms of radar scatter are critically affected by the surface roughness properties, the research of CG waves is of special interest to ocean remote sensing.

Field acquisition of CG wave data has been difficult due to (1) high Doppler frequency shift by current advection, rendering controversial interpretation of the point measurements; (2) spatial measurements using wave gauge arrays are limited by frequency response and error due to meniscus effects; and (3) quantitative inversion of the images of optical scattering from a random surface is complicated, and the nonuniform ambient lighting condition encountered in the field further contribute to the difficulties of retrieving the surface roughness structure from optical images.

In order to overcome these problems, spatial measurement techniques suitable for field application are needed. Section 2 presents a scanning slope sensing method for performing spatial measurements of short water waves. Section 3 demonstrate the ability of the scanning slope sensor to acquire high resolution measurements on the spatial and temporal evolution of CG waves propagating on the water surface. Section 4 summarizes the results and discussion.

2. OPTICAL SCANNING SLOPE SENSING

A. Design concept

To measure CG waves, laser slope sensors based on optical refraction were used in the past for their high frequency response and high resolving power of the fine structure at the water surface (1-6). The typical design projects vertically a laser beam from underwater. As the beam intersects the air-water interface, the optical path changes due to differences in the refraction indices of air and water. The refraction of the light beam from water to air follows Snell's law of wave propagation. Thus by monitoring the position of the refracted beam, the surface slope at the position of the laser beam penetration can be derived. Note that although from the optical consideration it is preferred to have the laser beam project from air to water, reversing the projection path has the definitive advantage of reducing ambient light effect on the receiver in the field application.

Single-point slope sensors, however, provide only time series of the surface fluctuation and frequency spectra of short waves. It is difficult to resolve the length scale from time series or frequency spectra because convection of short CG waves by surface currents produces a large Doppler frequency shift. In order to obtain wavenumber resolution, direct spatial measurements are needed. The laser slope sensing technique can be modified such that instead of dwelling at a fixed point, the laser beam scans rapidly across the water surface. If the scanning speed is sufficiently higher than the wave motion, the surface can be considered frozen, producing effectively a spatial measurement of the surface fluctuation (7). This approach is attractive because the operation principle is still based on the refraction of a single laser beam. The signal interpretation is straight forward. Furthermore, with simple scanning patterns (for example, linear or rectangular grids), the data analysis procedures such as one-dimensional and two-dimensional Fourier Transformations are well developed.

In the following, the fundamental relationship of the single-beam refraction technique is described first, followed by a discussion of scanning slope sensing and a description of related hardware components.

B. Optical refraction technique

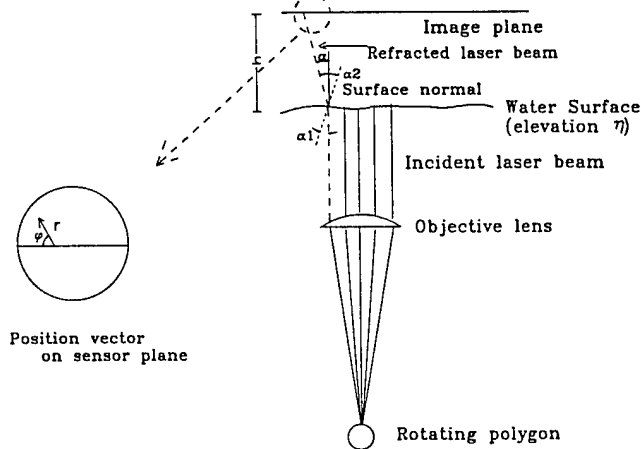Referring to Fig. 1, the angles of the incident and refracted beams are related by Snell's Law

Figure 1. A sketch showing the refraction of a laser beam crossing the air-water interface. The surface slope can be derived from the position vector of the refracted laser beam.

$$n_1 \sin \alpha_1 = n_2 \sin \alpha_2 \qquad (1)$$

where n is the refractive index, α is the angle between the beam path and the surface normal, and subscript 1 is for water and 2 for air. From the above relationship, the slope of the water surface can be derived from the position of the refracted beam on an imaging surface at a given distance from the air-water interface. This is the basic principle used in most optical surface slope measuring devices, many of them also include a lens positioned at the focal distance in front of the imaging plane to direct parallel lights to the same location on the imaging surface. The addition of the lens is to insure that the determination of surface slope is not affected by the vertical fluctuations of water surface. When the laser beam scans over a finite segment, say, on the order of 10 cm, the required aperture of the lens to capture the refracted laser beam becomes quite large. Large aperture lenses are not only difficult to procure, they are also much more expensive. The added size and weight also increase the complication of a field system. Fortunately, the use of a focusing lens in the receiver module is a convenience rather than necessity. If a focusing lens is not used, the surface fluctuation needs to be measured and incorporated into the formula to derive the

surface slope. Referring to Fig. 1 again, the angle between the vertical and the refracted beams is uniquely determined by

$$\alpha = \tan^{-1} \frac{r}{h + \eta} \qquad (2)$$

where h is the distance between the imaging plane and the mean water surface, η the instantaneous surface displacement, and r the magnitude of the position vector, r, of the refracted beam on the image plane. The surface slope with respect to the horizontal plane, $s = |\nabla \eta| = \tan \alpha_1$, can be obtained from (1), i.e.,

$$\tan \alpha_1 = \frac{0.75 \sin \alpha}{1 - 0.75 \cos \alpha} \qquad (3)$$

where $n_1 = 4/3$ and $n_2 = 1$ were substituted. The azimuthal angle, ϕ, of the surface tilt is the same as that of the position vector r. Conventionally, the surface slope is expressed in terms of its two orthogonal components $\eta_x = s \cos \phi$ and $\eta_y = s \sin \phi$.

C. Instrument components

1) Scanner

Scanning of the laser beam can be accomplished by using an acousto-optic modulator (AOM) or a scanning mirror (SM). The former offers the advantage of precise control of laser beam positions in digital steps, and was used in a laboratory system (8). Because sufficient details have been presented in (8), it is briefly noted here that the AOM was programmed to project 60 positions along a 11.6-cm line segment with a repetition rate of 200 scans per second. Two major difficulties are encountered when trying to extend this design to field application: (a) The diffraction efficiency of an AOM is low, thus requires an expensive laser source; and (b) The diffraction angle using an AOM is small, typically on the order of one to two degrees, and therefore the design would require a more complicated optical system or a rather long optical path between the AOM and the water surface in order to achieve a reasonable scanning distance at the air-water interface. To resolve these difficulties in field operation, laser scanning was accomplished by using a rotating polygon mirror (SM) in the field system (7). To create a telecentric and collimated sheet of laser beam, a double-pass pre-objective scanning design is adopted (9-10). As shown in Fig. 2, the laser beam is introduced from the exterior of the objective lens to be focused on the scanning polygon placed at one focusing length from the lens. The laser beam is then reflected by the mirror facets of the

rotating polygon. The reflected beams are then collimated by the object lens and projected to the scanning region at the water surface. The diameter and focal length of the object lens are 15 and 40 cm, respectively. For the 10 cm scanning distance, the effective f-number of the lens is 4.
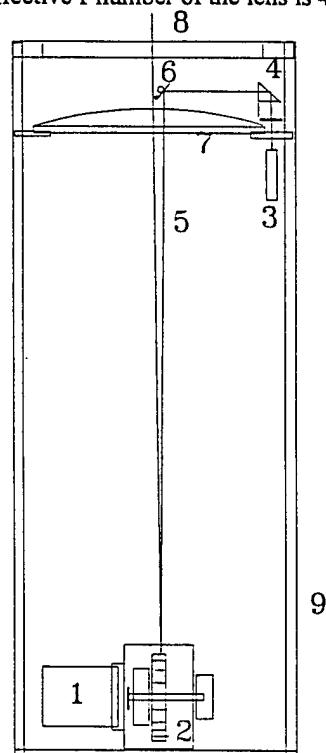

Figure 2. The double-pass, pre-objective design for producing a telecentric collimated scanning laser sheet. The direction of the scanning laser line is into the page. The components identified in the figure are: 1: motor, 2: polygon mirror; 3: diode laser; 4: prism; 5: laser beam path; 6: mirror; 7: object lens; 8: window; and 9: water-tight case.

The key element determining the scanning pattern is the rotating polygon mirror. To allow for a 10-cm scanning distance at the position of the objective lens from the focal point, the angle of each facet is calculated to be approximately 7 degrees. Allowing for a factor of two duration to accommodate sampling of additional parameters such as wind, wave, temperature, ambient light, a 24-sided polygon mirror is selected. For the one-dimensional scanning, the angles in the cross-scan orientation (hereafter referred to as the cross-scan angle) of the 24 facets are identical. To create a two-dimensional scan of 8 lines spaced 5 mm apart, the 24 facets were cut into three sets of 8 different cross-scan angles in steps of 0.36 degree. The polygon mirror is mounted on the shaft of a variable speed DC motor, which has a maximum rotating speed of 30,000 rpm. At this maximum rotating speed, the line repetition period for a 24-sided polygon mirror would be 2 ms, or 16 ms

for a 8-line frame. As will be discussed in the next section, the system response is limited by other hardware components, and this maximum scanning performance was not used.

2) Receiver

The principal component of the receiver module is a two-dimensional position sensor (UDT PIN-SD/50) that records the instantaneous position of the refracted laser beam on the image plane. The frequency response of the position sensor is 70 kHz based on manufacturer's specification. Designed for a dynamic range of $\pm34°$, a frosted glass of 25 cm diameter is used as the scattering surface for imaging of the refracted beam. A 50 mm, f1.4 camera lens is used to focus the optical image onto the two-dimensional position sensor, which has a 4.45 cm diameter sensing surface. A pair of high pass and low pass filters are placed in front of the camera lens, and serve as a band-pass filter to reduce unwanted ambient lights. The bandwidth of the band-pass filter is 50 nm and the central wavelength is 675 nm. The wavelength of the diode laser used as the optical source is 670 nm. The signal from the position sensor is processed through two UDT 301DIV-30 kHz amplifiers to produce the (x, y) position output.

C. System response

For the laboratory system, the frequency response of the position sensor amplifier (30 kHz) is the limiting factor determining the scanning configuration. As mentioned earlier, the AOM was programmed to scan 11.6 cm in 60 equally-spaced positions with a 200 Hz line repetition rate. For the field system, the frequency response is limited by the A/D hardware (20 kHz) available for the AMPRO computer at the time of system fabrication (1991). Using two A/D interface cards, this digitization speed is sufficient for the design of one-dimensional scanning with a 5 ms line-repetition period and 50 sampling positions along a 10 cm scanning distance. When the linear scanning was modified to 8-line two-dimensional scanning, the A/D hardware was not changed. By slightly increasing the line-scan rate (decreasing the scanning period from 5 to 4.3 ms), the repetition rate of each two-dimensional pattern is approximately 29 frames per second, very close to the frame rate of a consumer video system. Of the 4.3 ms line repetition period, 2.5 ms is the actual optical scanning duration (that is, the duration that is sampled to obtained surface slope data), the remaining is used for collecting auxiliary measurements. With the above operational parameters, the optical scanning speed is 23.2 m s^{-1} for the laboratory system and 40 m s^{-1} for the field system, both figures are significantly faster than the advection speed

of capillary-gravity waves, and the surface can be considered frozen during the sampling of each scan. The laser scanning slope technique is the equivalence of placing multiple laser slope gauges in very high density. For example, the laboratory system described above is the equivalence of 60 gauges in a 11.6 cm linear segment, and the field system of 8-line, 50-spacing is the equivalence of 400 laser probes in a $4 \times 10 \text{ cm}^2$ area.

It is clear that for the laboratory setup, the dynamic range can be increased significantly because improvement on the optical aperture, electronic circuits and data acquisition speed can be easily accommodated, as the space restriction, a key factor for field systems, is typically not a consideration. Limitation on the data storage is also much less serious in the laboratory than in the field. Finally, the problem of ambient light contamination due to sun light in the field (7) is almost trivial in the laboratory; one needs only to turn off the lights in the laboratory, while night time operation in the field is potentially risky.

The optical sensor also records the ambient light intensit at the rate of linear scanning (nominally 200 Hz). Thi ambient light information is critical for the post-experimer data processing to compensate for the attenuation of positio signal due to ambient light (7). Other sensors to monito various environmental properties, such as wind, wave, an temperature, are also installed on both laboratory and fiel systems. The discussion of these sensors and other detaile of the field system is given in Hwang et al. (7,8).

3. LABORATORY AND FIELD MEASUREMENTS

A. Space-time evolution of wind waves

The scanning slope sensing technique is applied to study the spatial and temporal evolution of small-scale CG waves. Fig. 4 shows an example of the space-time images of the wave patterns at six different wind speeds in a straight wind-wave facility. For clarity of display, the image intensity at each wind speed has been normalized by the range (maximum minus minimum intensity) of the data in the given wind condition. All the data were collected at the fetch of 16 m. More details of the experimental conditions are reported in (8). The lowest wind speed selected ($u_* = 11 \text{ cm s}^{-1}$) corresponds closely to the incipient condition of short wave generation at this facility, the most prominent waves on the water surface are very regular waves with period of approximately 0.16 s (Fig. 3a). The range of wavelengths becomes much broader in the next higher wind speed ($u_*=17$

cm s^{-1}, Fig. 3b). The generation of CG wave packets appears to be intermittent, as shown in the 4-s data record in Fig. 3b, puffs of waves occurred at several locations (e.g., at $t \approx 0.8$, 1.0 and 3.5 s). The wavelengths of individual wave components in the packet range from a few millimeters to longer than 10 cm (based on the observed maximum period of 0.5 s in this record, the maximum wavelength is close to 40 cm). The shorter waves of the packet quickly dissipate, leaving only low frequency undulation on the water surface after each puff event. This observation is qualitatively consistent with the theoretical prediction of the modules of decay (11); the decay time scale is calculated to be longer than 20 minutes for a 30-cm wavelength component and 0.5s for a 0.63-cm wavelength component. At this wind speed, the interval between two major wave packets is approximately a few seconds. Smaller puffs of wave packets occur between these larger events at irregular intervals and with variable intensities. More detailed statistics are not possible due to the
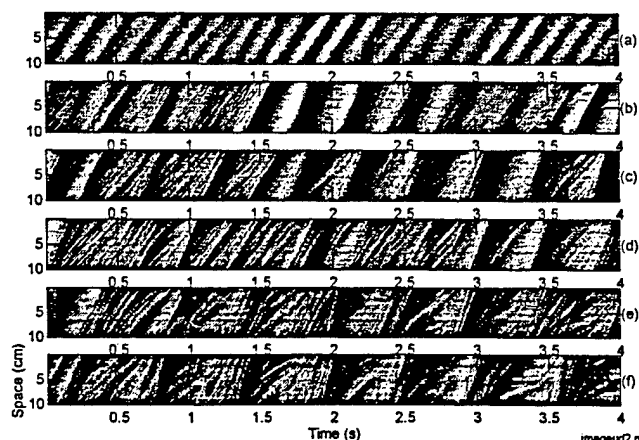

Figure 3. Space-time series of the surface slopes of wind-generated waves at 6 different wind speeds. The wind friction velocities are 11, 17, 23, 33, 43 and 54 cm/s (a to f).

At the next higher wind velocities ($u_*=26 \text{ cm s}^{-1}$, Fig. 3c), the generation of wind-wave packets becomes more regular, with distinct wave packets occurring near each wave crest. Unfortunately, the data file of surface elevation of this series of experiments was lost. Additional discussion of phase distribution along long waves is given in the modulation experiments to be described in the next section. Quite interestingly, the simultaneous measurement of radar backscatter also indicated major increase of radar sea spikes at this wind speed of $u_*=26 \text{ cm s}^{-1}$ (12). For the next three wind speeds (Figs. 3d to 3f), the patterns of the CG wave distribution on the water surface are similar, showing distinctive modulation by the background short gravity waves.

The wavelengths range of the CG wave components in each packet become broader and the intensity of events become more active as wind speed increases. From these space-time images, it is clear that the group velocity of short waves of sub-centimeter wavelength is significantly modulated by the underlying longer wave components. The propagation velocity can be estimated from dx/dt, where dx is the distance traveled following the wave component, and dt is the time interval. For example, in the wave packet at the vicinity of $t = 3.5$ s of the second wind speed case, the group velocity of the wave components with similar length scales may vary from less than 10 cm s^{-1} to almost 1 m s^{-1}. The wavenumber spectra can be derived from these direct spatial measurements of the surface undulation; the results are reported in (8).

B. Modulation

To study the modulation of short waves by surface currents, mechanical waves can be added to the wind-wave system. Fig. 4 shows an example of the modulated surface roughness patterns captured by scanning slope sensing. The period of the monochromatic wave train is 1 s. In these plots, the surface slope images were processed with conditional sampling based on the phases of the mechanical waves, which were measured at the same fetch and aligned (with a lateral offset of 5 cm) with the mid-position of the scanning segment. Using the downward zero-crossing of the surface elevation as reference, the 1-s record immediately following the zero-crossing of mechanical waves is divided into 200 phases. The top panel (Fig. 4w) above the image strips plots the surface displacement records of the first three wind conditions. The surface slope pattern of each wind speed condition displays the repeating cycles of stretching and compressing. The highest density of short and steep waves is found to be in the windward phase of the crests of mechanical waves. (In these images, the directions of wind and mechanical waves are from right to left). For short wave components of similar wavelengths, the group velocities in the trough phase of long waves are clearly much slower than those near the wave crest region. At lower wind conditions, the propagation of short wave components can be traced easily from these space-time images. As wind speed increases, the surface roughness pattern becomes much more complicated but the repeating pattern of surface modulation by the mechanical waves remains quite distinctive.

Fig. 5. displays the phase distribution of the spectral density of short wind waves along the underlying mechanical waves. In these plots, the top trace is the distribution of

current strain dU/dx, calculated from $-\omega d\eta/dt/C$, where ω is the angular frequency, η the surface elevation and C the phase speed of mechanical waves. The second trace is the surface
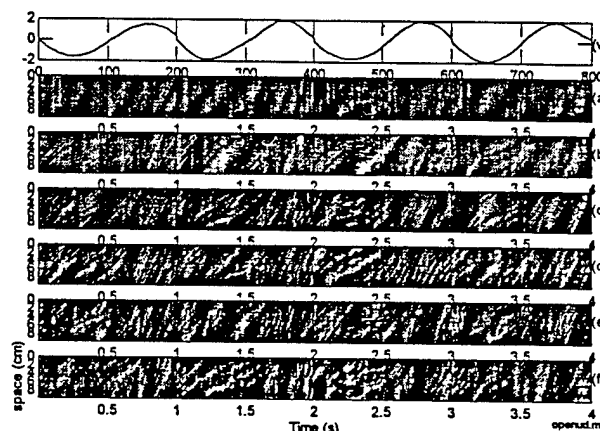

Figure 4. Modulation of short wind waves by ambient mechanical waves of 1-s period. The wind conditions are identical to those in Fig. 3 (a to f). The surface displacement, shown on the top of these images (labeled (w)), measured at the same location of the laser scanning is used for phase reference.

The remaining curves are the distribution of the spectral densities of particular wavenumbers, the magnitudes of which are scaled with the numbers (in rad cm^{-1}) labeled on the vertical axis (for the 11.6-cm scanning distance and 60 scanning positions, the range of wavenumbers resolved is 0.54 to 16.2 rad/cm). The phase distribution illustrates two major characteristics: (a) the modulation magnitude decreases with increasing wind stress and/or wavenumber, and (b) the modulation phase shifts from in-phase with surface elevation of mechanical waves for the longer modulated waves to in-phase with current shear for the shorter modulated waves. These properties are in qualitative agreement with the relaxation theory (13-15). Results on the hydrodynamic modulation transfer function calculated from the data shown in Figs. 4 and 5 are given in (16).

C. Two-dimensional wavenumber spectrum

As discussed earlier, the scanning method can be extended to two-dimensional coverage of the water surface without much difficulty. Reference (7) present the results obtained from a free-drifting scanning slope sensing buoy designed for field deployment.

The scanning pattern is rectangular and composed of 8 straight lines spaced 5 mm apart. Each straight segment is 10 cm long and sampled at 2 mm intervals. The resulting system is equivalent to placing 400 laser slope gauges in the 4×10 cm^2 surface area. An example of the two-dimensional surface

roughness structure of short wind waves is shown in Fig. 6. These images (at the acquisition rate of 29 frames per second) illustrates the rapid variation of the ocean surface waves in the capillary-gravity regime. Regions of steep hills and valleys are frequently observed.
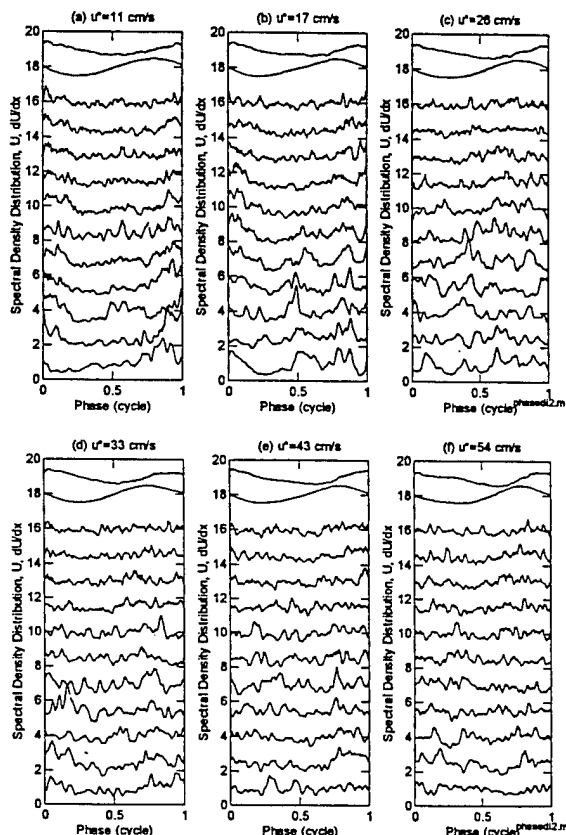

Figure 5. The phase distribution of the spectral densities of short water waves. The top trace represents the current shear, the second trace is the surface displacement. The remaining curves are the spectral density at different wavenumbers, the magnitudes of which scale with the numbers (i rad/cm) on the vertical axis. These curves are normalized by the mean values of the spectral densities (over all phases) of each wavenumber.

These steep regions in the surface geometry contribute 1 strong radar backscatter (sea spikes) from the ocean surface (12, 17, 18). From such images, the two-dimension wavenumber spectra can be calculated. The results for the six cases reported in (7) are plotted in order of increasing surface roughness in Fig. 7. For the lowest wind velocity case (1213, Fig. 7a, $U_{1.3} = 0.4$ m s^{-1}, where $U_{1.3}$ is the wind speed measured at 1.3-m elevation), there is very little structure in the two-dimensional wavenumber spectrum. The ocean surface was observed from the research vessel to be very smooth during this period. The next two cases (1810 and 2422, Figs. 7b and 7c) have essentially the same mean wind velocity ($U_{1.3} = 1.0$ and 1.1 m s^{-1}), but the wind fluctuations are much larger for case 2422. The environmental conditions

are further complicated by the presence of slick bands on the water surface on both days (7). In any event, the spectral intensities near the peaks of these two cases differ by a factor of 10.
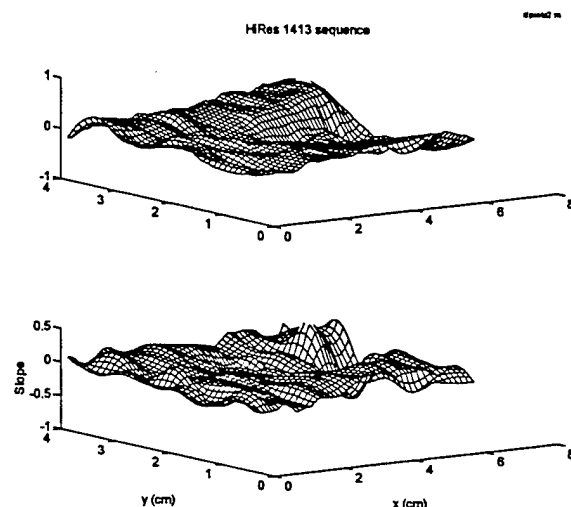

Figure 7. The two-dimensional geometry of sea surface slopes measured by a scanning slope sensor mounted on a free-drifting buoy (7). The data acquisition rate is 29 frames per second. The sequence of the frames is from left to right, and top to bottom.
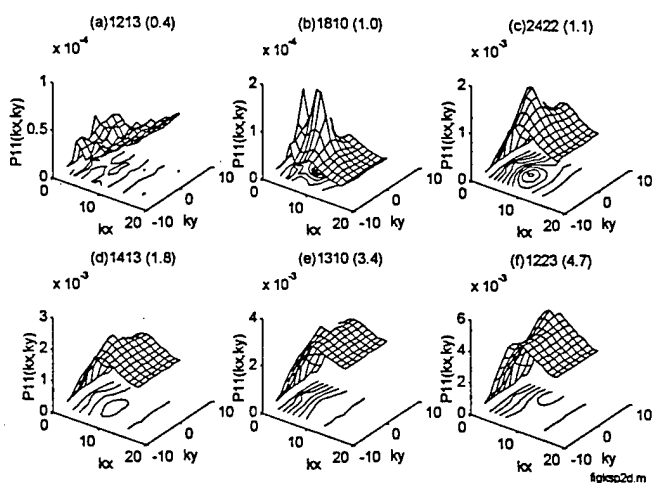

Figure 7. The two-dimensional wavenumber spectra of capillary-gravity waves measured by a scanning slope sensor mounted on a free-drifting buoy (7). The mean wind speed, measured at 1.3 m above the mean water level, of each spectrum is shown in parentheses on top of each plot.

The distribution of the two-dimensional spectral density is very narrow (i.e., very localized in the wavenumber domain), showing strong peaks near $k_x = 8$ rad cm^{-1}. As the wind speed increases, the spectral level continues to increase; at the same time, the directional distribution broadens. In general, the peak spectral energy aligns with the wind direction (along $k_y = 0$) with the exception of the last case (1223, $U_{10} = 5.7$ m

s^{-1}), where two local spectral peaks are found to be on the opposite sides of the mean wind direction. This may be an indication of bimodal distribution. From these two-dimensional wavenumber spectra, the directional distribution of individual short-wave components can be calculated. Examples of the results are shown in Fig. 8. There is an indication of progressive narrowing of the directional distribution toward higher wavenumbers for a given wind speed. For individual wavenumber components, there is a trend of broadening of the directional distribution toward higher wind speeds in the first four cases shown in this figure ($U_{1.3} = 1.0$ to 3.4 m s^{-1}). The wind dependence appears to be stabilizing: the distributions between the last two cases ($U_{1.3} = 3.4$ and 4.7 m s^{-1}) are almost identical for the three wavenumber components shown. A more quantitative study of the variation of directional distribution as a function of wavenumber and wind speed is in progress.

Note that there is an apparent offset between the directions of wave propagation and wind vector in all the cases presented in Fig. 8. This directional offset is due to the misalignment of the buoy orientation due to asymmetric wind and current loadings on the instruments mounted on the buoy structure. At lower wind conditions, the oscillatory wave-induced drag dominate the buoy orientation. The magnitude of the directional offset reduces toward higher wind speed, showing the effectiveness of the wind vane installed on the scanning slope sensing buoy for aligning the scanning direction with wind (7). This offset should not be interpreted as that the waves are not propagating in the wind direction. Additional discussions on the statistics of the mean square slopes and transect wavenumber spectra are given in (7, 19, 20).

4. SUMMARY

This article describes a scanning slope sensing technique to obtain spatial information of small-scale waves on the ocean surface. The technique was applied successfully in both laboratory and field. The scanning slope sensing proves to be capable of acquiring high-resolution data on the spatial and temporal evolution of short waves on the ocean surface. It also shows potential for detailed study of the hydrodynamic modulation of capillary-gravity waves caused by the variation of surface currents from miscellaneous features on the ocean surface.

The spatial measurements also provide direct computation of wavenumber spectra of the small scale ocean waves. Some preliminary results of the two-dimensional wavenumber

spectra were presented. There is a strong indication of progressive narrowing of the directional distribution toward shorter wavelengths for a given wind speed and gradual broadening of the directional distribution toward high-wind velocities for a given wavenumber.
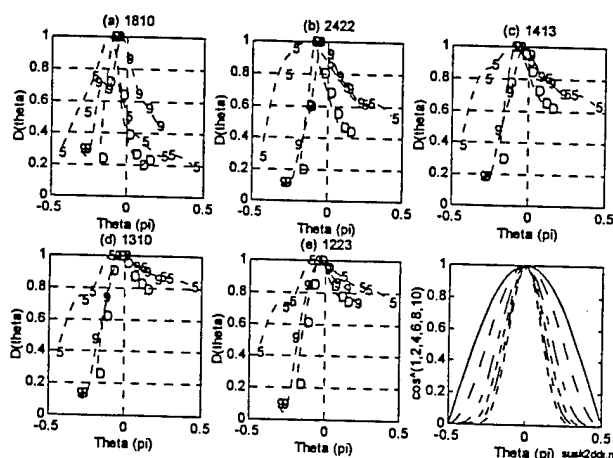

Figure 8. The directional distributions of the last five cases shown in Fig. 8. (a - e) The wavenumber components shown in each panel are $k = 5, 9$ and 13 rad cm^{-1} and are identified by the symbols "5", "9", and "D", respectively. (f) The function $\cos^n \theta$, with $n = 1, 2, 4, 6, 8$, and 10.

REFERENCES

[1] C. S. Palm, C. S., "An instrument to measure the two-dimensional wave slope spectrum of ocean capillary waves," Ph. D. Dissertation, Aeronautical Engineering, Univ. of Florida, 70 pp, 1975.

[2] B. A. Hughes., J. L. Grant, and R. W. Chappell, "A fast response surface-wave slope meter and measured wind-wave moment," Deep-Sea Res., vol. 24, pp. 1211-1223, 1977.

[3] C. S. Palm, C. S., R. C. Anderson, and A. M. Reece, "Laser probe for measuring 2-D wave slope spectra of ocean capillary waves," Appl. Opt., vol. 16, pp. 1074-1081, 1977.

[4] S. Tang, and O. H. Shemdin, "Measurement of high frequency waves using a wave follower," J. Geophys. Res., vol. 88, pp. 9832-9840, 1983.

[5] P. A. Hwang, and O. H. Shemdin, "The dependence of sea surface slope on atmospheric stability and swell conditions," *J. Geophys. Res.*, vol. 93, pp. 13903-13912, 1988.

[6] O. H. Shemdin, and P. A. Hwang, "Comparison of measured and predicted sea surface spectra of short waves," *J. Geophys. Res.*, vol. 93, pp. 13883-13890, 1988.

[7] P. A. Hwang, S. Atakturk, M. A. Sletten, and, D. B. Trizna, "A study of the wavenumber spectra of short water waves in the ocean," *J. Phys. Oceanogr.*, vol. 26, pp. 1266-1285, 1996.

[8] P. A. Hwang, D. B. Trizna, and J. Wu, "Spatial measurements of short wind waves using a scanning slope sensor," *Dyn. Atm. and Oceans*, vol. 20, pp. 1-23, 1993.

[9] L. Beiser, "Laser scanning systems," in *Laser Applications*, Vol. 2, Academic Press, pp. 53-159, 1974.

[10] R. E. Hopkins, and M. J. Buzawa, "Optics for laser scanning," *Opt. Eng.*, vol. 15, pp. 90-94, 1976.

[12] D. B. Trizna, J. P. Hansen, P. A. Hwang, and J. Wu, "Ultra wideband radar studies of steep crested waves with scanning laser measurements of wave slope profiles," *Dyn. Atm. & Oceans.*, vol. 20, pp. 33-53, 1993.

[13] W. C. Keller, and J. W. Wright, "Microwave scattering and the straining of wind-generated waves," *Radio Sci.*, vol. 10, pp. 135-147, 1975.

[14] B. A. Hughes, "The effect of internal waves on surface wind waves, 2. Theoretical analysis," *J. Geophys. Res.*, vol. 83, pp. 455-465, 1978.

[15] P. A. Hwang, and O. H. Shemdin, "Modulation of short waves by surface currents - a numerical solution," *J. Geophys. Res.*, vol. 95, pp. 16311-16318, 1990.

[16] P. A. Hwang, P. A., "Optical measurements of the structure of short water waves and their modulation by surface currents," in *Optics of the Air-Sea Interface: Theory and Measurement*, SPIE Proc. Vol. 1749, pp. 216-221, 1992.

[17] D. B. Trizna, J. P. Hansen, P. A. Hwang, and J. Wu, "Laboratory studies of radar sea spikes at low grazing angles," *J. Geophys. Res.*, vol. 96, pp. 12529-12537, 1991.

[18] L. Wetzel, "A time domain model for sea scatter, *Radio Science*, vol. 28, pp. 139-150, 1993.

[19] P. A. Hwang, "Spatial measurements of small-scale ocean waves," in *Air-Water Gas Transfer*, eds. B. Jahne and E. C. Monahan, AEON Verlag & Studio, Hanau, Germany, pp. 153-164, 1995.

[20] P. A. Hwang, "A study of the wavenumber spectra of short water waves in the ocean: Spectral model and mean square slope," subm. to *J. Atm. and Oceanic Tech.*, 1996.

REPORT DOCUMENTATION PAGE

Public reporting burden for this collection of information is estimated to average 1 hour per response, including the time for reviewing instructions, searching existing data sources, gathering and maintaining the data needed, and completing and reviewing the collection of information. Send comments regarding this burden or any other aspect of this collection of information, including suggestions for reducing this burden, to Washington Headquarters Services, Directorate for Information Operations and Reports, 1215 Jefferson Davis Highway, Suite 1204, Arlington, VA 22202-4302, and to the Office of Management and Budget, Paperwork Reduction Project (0704-0188), Washington, DC 20503.

1. AGENCY USE ONLY (Leave blank)	2. REPORT DATE October 1996	3. REPORT TYPE AND DATES COVERED Proceedings

4. TITLE AND SUBTITLE

Measurement of the Microstucture of Ocean Surface Roughness

6. AUTHOR(S)

Paul A. Hwang

5. FUNDING NUMBERS

Job Order No. 73-7075-06

Program Element No. 0601153N

Project No.

Task No.

Accession No.

7. PERFORMING ORGANIZATION NAME(S) AND ADDRESS(ES)

Naval Research Laboratory
Oceanography Division
Stennis Space Center, MS 39529-5004

8. PERFORMING ORGANIZATION REPORT NUMBER

NRL/PP/7332-96-0020

9. SPONSORING/MONITORING AGENCY NAME(S) AND ADDRESS(ES)

Office of Naval Research
800 North Quincy Street
Arlington, VA 22217-5000

10. SPONSORING/MONITORING AGENCY REPORT NUMBER

11. SUPPLEMENTARY NOTES

Proceedings of Microstructure Sensors Workshop, 23-25 October 1996, Timberline Lodge, Mt. Hood, Oregon

12a. DISTRIBUTION/AVAILABILITY STATEMENT

Approved for public release; distribution is unlimited.

12b. DISTRIBUTION CODE

13. ABSTRACT (Maximum 200 words)

This paper describes a technique to measure the spatial structure of short capillary-gravity waves in the ocean. The method is based on optical refraction of a single laser beam crossing the air-water interface to derive the surface slope information. By quickly scanning the laser beam, the spatial and temporal evolution of the surface undulation can be studied in great detail. The spatial measurement of the surface fluctuation also allows direct computation of the wavenumber spectrum in the capillary-gravity wave regime to avoid the difficulty of resolving the Doppler frequency shift as encountered in the processing of high frequency spectra derived from a single-point sensor.

14. SUBJECT TERMS

physical oceanography, microstructure, waves, gravity, optical refraction, laser beam, surface slope, Doppler, and remote sensing

15. NUMBER OF PAGES 10

16. PRICE CODE

17. SECURITY CLASSIFICATION OF REPORT	18. SECURITY CLASSIFICATION OF THIS PAGE	19. SECURITY CLASSIFICATION OF ABSTRACT	20. LIMITATION OF ABSTRACT
Unclassified	Unclassified	Unclassified	SAR